

# MOND in galaxy groups: A superior sample

Mordehai Milgrom

*Department of Particle Physics and Astrophysics, Weizmann Institute, Rehovot Israel 7610001*

Intermediate-richness galaxy groups are an important testing ground for MOND. First, they constitute a distinct type of galactic systems, with their own evolution histories and underlying physical processes; second, they probe little-chartered regions of parameter space, as they have baryonic masses similar to massive galaxies, and similar velocity dispersions, but much larger sizes – similar to cluster cores (or even to clusters), but much lower dispersions. Importantly in the context of MOND, they have the lowest internal accelerations reachable inside galactic systems. Following my recent analysis of MOND in galaxy groups, I came across a much superior sample, which I analyze here. This extensive catalog permits strict quality cuts that still leave a large sample of 56 medium-richness groups, better suited for dynamical analysis – e.g., in having a large number ( $\geq 15$ ) of members with measured velocities. I find that these groups obey the deep-MOND relation between baryonic mass,  $M_M$ , and velocity dispersion,  $\sigma$ :  $M_M G a_0 = (81/4)\sigma^4$ , with individual, MOND, mass-to-light ratios,  $M_M/L_K$  of order  $1 M_\odot/L_{K,\odot}$ , and a sample median value of  $(M_M/L_K)_{med} = 0.7 M_\odot/L_{K,\odot}$ . These compare well with stellar values deduced for single galaxies, and with values deduced from population-synthesis analyses. In contrast, the dynamical, Newtonian  $M_d/L_K$  values are much larger – several tens solar units, and  $(M_d/L_K)_{med} = 37 M_\odot/L_{K,\odot}$ . The same MOND relation describes (isolated) dwarf spheroidals – two-three orders smaller in size, and seven-eight orders lower in mass. The groups conformation to the MOND relation is equivalent to their lying on the deep-MOND branch of the “mass-discrepancy-acceleration relation”,  $g \approx (g_N a_0)^{1/2}$ , for  $g$  as low as a few percents of  $a_0$  ( $g_N$  is the Newtonian, baryonic, gravitational acceleration, and  $g$  the actual one). This argues against systematic departure from MOND at extremely low accelerations (as has been suggested). This conformation also argues against the hypothesis that the remaining MOND conundrum in cluster cores bespeaks a breakdown of MOND on large-distance scales; our groups are as large as cluster cores, but do not show obvious disagreement with MOND. I also discuss the possible presence of the idiosyncratic, MOND external-field effect.

PACS numbers: 04.50.Kd, 95.35.+d

## I. INTRODUCTION

Galaxy groups are important in testing MOND ([1], reviewed, e.g., in Refs. [2, 3]) – especially *vis à vis* the dark-matter paradigm. Such groups are a class of galactic objects distinct from others, such as dwarf spheroidals, massive galaxies, and galaxy clusters, with different histories of formation and evolution, different physical processes that affect their evolution, and possibly a different dynamical state. Such differences are expected to lead to disparate relations between baryons and dark-matter in the dark-matter paradigm, with strongly history-dependent present states (see e.g., Refs. [4, 5]). In contradistinction, MOND predicts strict relations between the baryons and the observed dynamics that are oblivious to history, as long as the system under study, be it a dwarf satellite, a galaxy, or a galaxy group, is in virial equilibrium.

Intermediate-richness groups (as distinct from galaxy clusters) also probe a different region of parameter space from what can be reached with other galactic systems. They have masses and internal velocities similar to massive galaxies, but are tens of times larger. They are similar in size to galaxy-cluster cores, but have much lower velocity dispersions. They thus have much lower internal accelerations than found in either galaxies or galaxy clusters. In fact – importantly in the context of MOND – their internal acceleration are the lowest accessible in

galactic systems, typically several times lower even than is typical in dwarf spheroidal satellites.<sup>1</sup> I will find no departure from the predictions of MOND in such groups, which argues against breakdown of MOND at extremely low accelerations – a possibility that was raised e.g., in Ref. [8] based on analysis of ultra-faint dwarf galaxies.

Because such groups are as large as cluster cores, or even as clusters, they help us pinpoint the reasons for the remaining MOND conundrum in clusters, and whether it is due to some breakdown of MOND at large distances – as has been suggested occasionally – or to some other attribute of clusters. The fact that MOND works well for the present sample, as I will find, means that it is not a question of system size.

In a recent paper ([9], hereafter Paper I) I analyzed MOND in small-to-intermediate-richness galaxy groups listed in the three compilations in Refs. [10–12], totaling 53 groups. While an advance over previous MOND analyses of galaxy groups, this study still leaves much to be desired. For example, most of the groups analyzed have only a small number of members with measured velocities, with only eleven groups having more than ten

---

<sup>1</sup> Such low accelerations have been probed in MOND, far outside galaxies, using weak gravitational lensing [6, 7], but only statistically for samples of galaxies, not individually.

measured velocities. It is greatly advantageous to analyze groups with a large number of observed member velocities, in order to mitigate some of the various uncertainties that beset the identification and analysis of groups, which assumes that they are bound, virialized, isotropic, isolated systems. Indeed, Paper I found clear-cut agreement with the predictions of MOND for the groups with more than 10 measured velocities, while those with a small number of velocities show large scatter.

In the meanwhile, I came across an earlier, much more extensive compilation Ref. [13] that identified 365 galaxy associations as “galaxy groups”. This large pool allows the application of “quality cuts” that still leave a large subsample of groups better suited for dynamical analysis.

Here, I use the subsample of groups in Ref. [13] with at least 15 members with measured velocities, and, furthermore, I leave out the (ten) groups at the very-rich end of the sample, to avoid having to account for the large contribution to the baryonic mass of hot gas these rich-groups/clusters are known to harbor. I then repeat the analysis as described in Paper I for the remaining subsample of 56 groups.

Galaxy groups were first analyzed in MOND in the very first MOND trilogy [14], where, however, only a small number of groups with reasonable number of observed radial velocities were available (only 5 would have pass our cut here). Also, the deep-MOND virial relation we now use for analyzing groups was not known at the time. In Ref. [15], I analyzed four group catalogs, but given only the published averages and median values of the luminosities and velocity dispersions for these catalogs, with no analysis of individual groups. In Ref. [16], I considered a small sample of 8 relatively nearby groups from Ref. [17]. Most of these groups have dynamical times comparable with the Hubble time; so it is questionable whether they are in virial equilibrium, and four of them had no more than 4 members with measured velocities. Testing MOND in pressure-supported galactic systems, Ref. [18] plots for the first time (in its Figure 7) the MOND “acceleration-discrepancy relation” – also known as the “mass-discrepancy-acceleration relation (MDAR) – for such systems; it shows also some groups (with very large scatter). All these analyses gave results consistent with MOND.

In Sec. II, I describe details of the analysis: the method used and the choice of subsample for analysis. In Sec. III, I describe the results, including a comparison with previous similar analysis of dwarf-spheroidal satellites of Andromeda. Section IV discusses the results and lists some known sources of uncertainties and scatter about the MOND relation.

## II. ANALYSIS

### A. Method

The MOND relation used to analyze the groups was described in detail, including the associated caveats, in Paper I. Here I recap the method, and comment on additional aspects not discussed in Paper I. The caveats and known sources of systematics – some of which are specific to the present sample – are discussed in Sec. IV A.

The starting MOND relation is ([19] and references therein)

$$\langle\langle(\mathbf{v} - \mathbf{v}_0)^2\rangle\rangle_t = \frac{2}{3}(MGa_0)^{1/2}\left[1 - \sum_i (m_i/M)^{3/2}\right], \quad (1)$$

where  $\mathbf{v}$  is the three-dimensional velocity,  $\mathbf{v}_0$  is the center-of-mass velocity,  $\langle\rangle$  is the mass-weighted average over the constituents, whose masses are  $m_i$ ,  $\langle\rangle_t$  is the long-time average, and  $M$  is the total mass. Relation (1) applies to isolated systems (ideally of point masses), deep in the MOND regime.

The groups I shall consider here are all very deep in the MOND regime. Assuming long-term stationarity – which requires boundedness (but is not ensured by it) – we replace the long-time average with the measured present-day value. The three-dimensional velocity dispersions is replaced by  $\sqrt{3}\sigma$ ,  $\sigma$  being the line-of-sight component – the only one that is measured. This assumes global velocity isotropy – a strong assumption that is not valid, for example, if rotation is important. For determining masses we use literature values of  $\sigma$ , which are not mass weighted ones, as appear in relation (1), and in any event are measured only from radial velocities of (usually small) subsample of system members.

Since individual masses of all members are not known, one usually uses relation (1) for the case of a system made of  $N \gg 1$  masses individually  $\ll M$ , in which case we get

$$M \approx \frac{81}{4}\sigma^4(Ga_0)^{-1}. \quad (2)$$

This is the approximate relation used in Paper I (and, e.g., in analysing the MOND dynamics of Andromeda satellites in Refs. [20, 21]; see also the application in Ref. [22] to the MOND analysis of elliptical galaxies). Here, I shall purposely consider only groups with at least 15 members with measured velocities (and possibly many more members); so the finite- $N$  correction is not large if, indeed, all masses are small compared with  $M$ . But,  $N \gg 1$  does not ensure the validity of relation (2). For example, in the case of one very dominant mass,  $M$ , with all the rest consisting of “test particles”, relation (1) reads, given the above approximation for the left-hand side,

$$M \approx 9\sigma^4(Ga_0)^{-1}, \quad (3)$$

where  $\sigma$  is the mass weighted dispersion of the test particles alone. This gives masses that are a factor of 9/4

smaller than from eq. (2) (or  $\sigma$  values  $\approx 20\%$  larger, for a given mass).

In the present analysis, I use the sample of groups described in Sec. II C, with group parameters as given in Ref. [13], which I list in Table I. They are: the numbers of member galaxies with observed radial velocities,  $N_V$ ; the line-of-sight velocity dispersions,  $\sigma$ , deduced from the measured radial velocities; the harmonic radii,  $R_h$ ; the K-band luminosities,  $L_K$ ; the Newtonian, dynamical masses,  $M_d$ ; and the corresponding Newtonian mass-to-light ratios,  $M_d/L_K$ . For each group, I calculate from  $\sigma$  the MOND baryonic mass,  $M_M$ , using eq. (2), and the corresponding mass-to-light ratio,  $M_M/L_K$ , to be compared with reasonable baryonic values. I also reverse the procedure and calculate the expected MOND velocity dispersion,  $\sigma_M$ , using eq. (2), from the given luminosity and assuming a fiducial value of  $M(\text{baryon})/L_K = 1 M_\odot/L_{K,\odot}$ . All these are also given in Table I.

## B. Alternative forms

The deep-MOND  $M - \sigma$  virial relations of the type discussed above are the proper MOND predictions to be tested in “pressure-supported systems” such as the groups. They do not require knowledge of sizes – a direct result of the scale invariance of the deep-MOND limit [23]. Such relations can, however, be cast in a form that resembles the acceleration-discrepancy relation – the basic MOND prediction for circular orbits in an axisymmetric field [1, 24], as relevant to rotation curves of disc galaxies<sup>2</sup> – by introducing some characteristic system radius,  $\bar{R}$ , which is needed for the definition of accelerations.

As explained in Ref. [25], despite their similar appearance, the global  $M - \sigma$  relations are different and independent MOND predictions from the local, mass-asymptotic-speed relation  $V_\infty^4 = MG a_0$ . (For example, the former is valid only for systems wholly in the deep-MOND regime, the latter is valid for all systems.) The latter is, in fact, a corollary of the former for the case of a test mass on a circular orbit around a central (baryonic) mass  $M$ . The  $M - V_\infty$  relation is tantamount to the “acceleration-discrepancy relation” between the observed (MOND) acceleration  $g = V_\infty^2/R$ , and the Newtonian acceleration  $g_N = MG/R^2$ :  $g = (a_0 g_N)^{1/2}$ , at all radii on the asymptotic rotation curve. MOND has extended this relation also to the interiors of disc galaxies at locations where  $g \ll a_0$ .

To write the  $M - \sigma$  relation in terms of “global” acceleration parameters, take, as an estimate of the global

Newtonian acceleration,

$$g_N = M_M G / (\kappa \bar{R})^2 \quad (4)$$

( $M_M$  is the MOND mass as defined above, because it stands for the baryonic mass), and the global true (MOND) acceleration as

$$g = \beta \sigma^2 / \bar{R}, \quad (5)$$

then, eq. (2), for example, can be written as

$$g = \eta (a_0 g_N)^{1/2}, \quad \eta \equiv 2\beta\kappa/9. \quad (6)$$

Since  $\kappa$  and  $\beta$  have values of a few,  $\eta \approx 1$ , and thus  $g \approx (a_0 g_N)^{1/2}$ .

Alternatively, we can write the ratio of the Newtonian to the baryonic (i.e., MOND) masses – which is also a measure of the mass-, or acceleration-discrepancy – in terms of  $g$ , as follows: Take an estimate of the Newtonian, dynamical mass to be such that

$$\frac{M_d G}{(\lambda \bar{R})^2} = g = \frac{\beta \sigma^2}{\bar{R}}, \quad (7)$$

for some  $\lambda$  of order 1. Then, with the above definitions

$$\frac{M_d}{M_M} = \frac{4\beta^2 \lambda^2 a_0}{81 g}. \quad (8)$$

Again, since  $\beta$  and  $\lambda$  have values of a few, this translates to  $M_d/M_M \approx a_0/g$ . I shall also compare the groups data with this relation.

## C. The sample

Putative groups with a small number of observed velocities,  $N_V$ , are not suitable for dynamical analysis; e.g., because they are likely to be chance, projected groupings and not bound, virialized groups (a caveat also pointed to in Ref. [13]); and because, even if the group itself is real, the resulting line-of-sight velocity dispersion may not be a good representation of the true, three-dimensional dispersion. A large number of group members (of which  $N_V$  is some measure) is also needed to justify the use of eq. (2).

The catalog of 365 galaxy ensembles cataloged in Ref. [13] as groups is large enough to allow quality cuts that still leave a large sample to be analyzed. Somewhat arbitrarily, I keep for analysis here only those groups with  $N_V \geq 15$ , totaling 67 groups. (Seven groups of those considered in Paper I have  $N_V \geq 15$ .) These groups are all listed in Table I with the parameter values assigned to them in Ref. [13] and the ones I calculated here.

I also want to exclude from the analysis galaxy clusters and rich groups that contain large quantities of x-ray emitting hot gas. The reason for this is twofold. First, if stars are not the dominant contribution to the baryonic

<sup>2</sup> Also known as the mass-discrepancy-acceleration relation (MDAR), aka “radial-acceleration relation” (RAR).

mass, the  $M/L$  ratios are not good indicators of the acceleration discrepancies, and the analysis must take into account the gas; but this is beyond the scope of the present analysis. Second, we already know from past analyses, for example in Ref. [26], that in such hot-gas-rich groups, MOND does not fully account for the discrepancies, and may require an additional baryonic contribution that we have not yet detected. This added so called “cluster baryonic dark matter”, may in fact be part and parcel of the hot gas [27], since, to my knowledge, such remaining MOND discrepancies are only seen in systems with substantial amounts of hot gas.

To bypass the need to check the individual groups systematically for the quantities of gas present, I – again somewhat arbitrarily – excluded from the final analysis the ten groups with  $N_V > 50$ .

For example, the group around NGC 4472 (M49), with the largest  $N_V$  is deep in the virgo cluster. The second group, “NGC 3311”, is the Hydra I cluster (Abel 1060), whose baryons are dominated by hot gas [28, 29]. The group “NGC 4696” is Centaurus. The group “NGC 3223” is the Antlia cluster, which is known to be hot-gas dominated [30]. The group “NGC 5044” is also known to be gas rich, with gas dominating the baryonic mass; it is one of the groups studied in MOND in Ref. [26]. The group “NGC 4261” is also hot-gas dominated [31].

As seen in Table I, some of these rich groups show reasonable MOND  $M_M/L_K$  values, but generally they have values considerably larger than  $1 M_\odot/L_{K,\odot}$ , which would be at least partly explained by the contributions of gas to the MOND baryonic mass.

In addition, I excluded one more group, “NGC 4216”, which Ref. [13] explicitly disqualifies (with several others that are not in my sample anyway) as having a very wrong assigned distance. I discuss and exemplify this issue in more detail in Sec. IV A.

All this leaves us with a sample of 56 groups (five groups of those considered in Paper I would remain after the second cut).

While the ten rich groups/clusters, and “NGC 4216”, with their resulting MOND quantities are shown in Table I, they are excluded from the plots in Sec. III.

### III. RESULTS

Using the  $\sigma$  values given in Ref. [13], I calculate the MOND masses of the groups,  $M_M$ , from eq. (2), and the resulting K-band mass-to-light ratio using the group K-luminosities from Ref. [13]. The distribution of these  $M_M/L_K$  values is shown in Fig. 1, to be contrasted with the distribution of Newtonian, dynamical values  $M_d/L_K$  (from Ref. [13]), shown in Fig. 2. While the Newtonian values are typically several tens solar units, and require the groups to be heavily dark-matter dominated in Newtonian dynamics, the MOND values are typically a factor of 40 smaller, and fall around 1 solar unit, with a median value of  $0.72 M_\odot/L_{K,\odot}$  (compared

with  $37 M_\odot/L_{K,\odot}$  for the Newtonian values). The distribution of  $M_d/M_M$  is shown in Fig. 3, with its median value of  $(M_d/M_M)_{med} = 41$ .

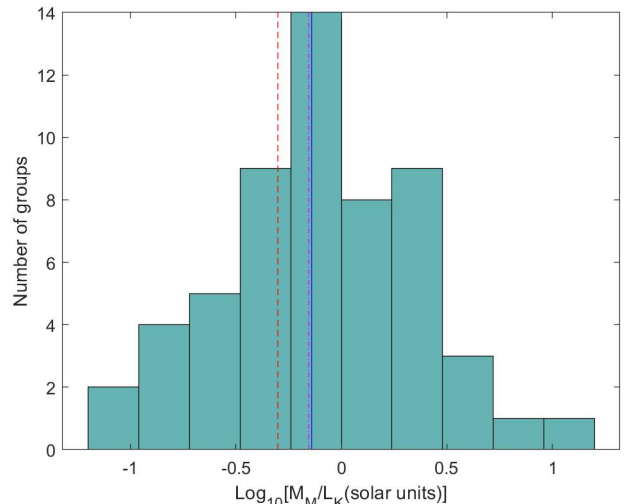


FIG. 1: The distribution of MOND dynamical  $M_M/L_K \equiv (81/4Ga_0)(\sigma^4/L_K)$  for our sample. The solid (blue) vertical line marks the sample median value of  $0.72 M_\odot/L_{K,\odot}$ . The dash-dotted (magenta) line, near it, is the value given in Ref. [32] for bulges (0.7), and the dashed (red) line is their value for discs (0.5), both deduced from MOND fits to rotation curves for the 3.6 micron photometric band. (See text for the small correction in comparing the two photometric bands involved.)

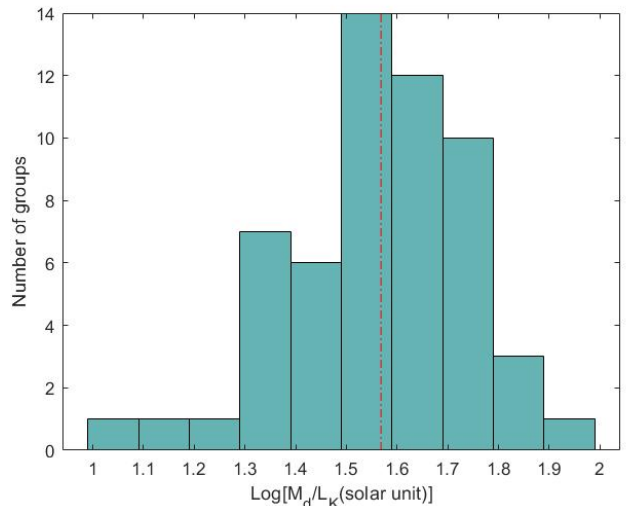


FIG. 2: The distribution of Newtonian, dynamical  $M_d/L_K$  ratios as derived in Ref. [13] for the groups in our sample. The dash-dotted (red) vertical line marks the median value of  $37 M_\odot/L_{K,\odot}$ .

Inasmuch as the baryonic masses of the groups is dominated by stars, these MOND mass-to-light ratios should agree with what is known and what is expected of stel-

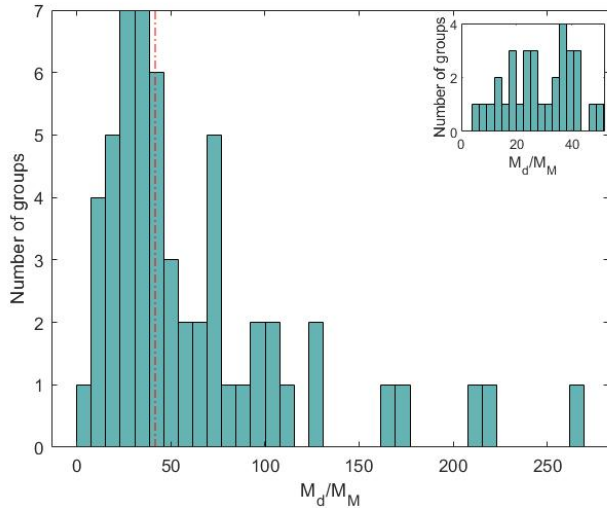


FIG. 3: The distribution of the Newtonian-to-MOND mass ratios  $M_d/M_M$ , with the median value of 41 marked by the vertical dash-dotted line. The inset is a closeup for small values.

lar  $M/L_K$  ratios, for example with what is deduced from population-synthesis models, or better yet, from the stellar  $M/L_K$  values directly deduced from rotation-curve analysis of individual galaxies.

Indeed, the distribution of the baryonic, MOND  $M_M/L_K$  values deduced here for the groups, and shown in Fig. 1, is very similar to those found for stellar values of discs and bulges in Ref. [32] (their Fig. 3) from rotation-curve analysis of many disc galaxies.<sup>3</sup> The group distribution is centered at nearly the same values, but is somewhat wider, as expected from the sources of scatter that are hardly present in rotation-curve analysis (such as interlopers, anisotropies, etc. – see Sec. IV A). These MOND mass-to-light ratios also agree with earlier analyses of rotation curves (e.g., [34], their Fig. 2), and with model calculations based on population synthesis (e.g., Ref. [35]).

It is worth reversing the procedure; namely, assume  $M/L_K = (M/L_K)_0$  for some reasonable reference value. Then calculate from eq. (2) the MOND-predicted values,  $\sigma_M$ , from  $L_K$ , to be compared with the measured  $\sigma$ . I do this with  $(M/L_K)_0 = 1 M_\odot/L_{K,\odot}$ , and show  $\sigma_M$  in Table I, together with  $\sigma_M/\sigma$ . By the definitions,

$$\sigma_M/\sigma \equiv [(M/L_K)_0/(M_M/L_K)]^{1/4} \quad (9)$$

Figure 4 shows the distribution of  $\sigma_M/\sigma$ , which has the same content as Fig. (1), but allows a more direct

comparison with the measured line-of-sight dispersions in consideration of the question marks that are known to beset these values (sampling, anisotropies, departure from virialization, inappropriate averaging of measured velocities – see Sec. IV A).

The median of the  $\sigma_M/\sigma$  distribution, which is indicated in various figures below, is clearly  $med(\sigma_M/\sigma) = [med(M_M/L_K)]^{-1/4} = 1.085$ . It is important that it is near 1, but its exact value is not so significant and follows from my choice to calculate  $\sigma_M$  from  $L_K$  using  $(M/L_K)_0 = 1 M_\odot/L_{K,\odot}$ . From eq. (9), the resulting value of  $med(\sigma_M/\sigma)$  scales as  $(M/L_K)_0^{1/4}$ .

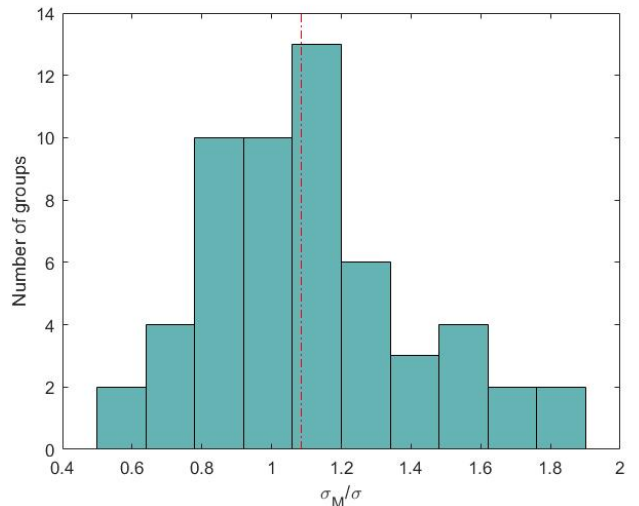


FIG. 4: The distribution of  $\sigma_M/\sigma$  (on a linear scale). The vertical dash-dotted (red) line marks the median value of 1.085.

Individual group are represented in the  $L_K - \sigma$  plane in Fig. 5 (with  $L_K$  and  $\sigma$  from Ref. [13]). Also shown are the MOND predictions of eq. (2) for several values of the mass-to-light ratios.

Five groups in the sample of Paper I pass our cuts here. They are also in the present sample. They are “NGC 3607”, “NGC 3379”, and “NGC 3627”, with parameters in Paper I taken from Ref. [11], and “NGC 5746” and “NGC 5363” with Paper-I parameters from Ref. [12]. Their positions in the  $L_K - \sigma$  plane are also shown in Fig. 5 with their parameters from Paper I; they are connected to their positions for the parameters from Ref. [13]. This comparison gives some notion of the uncertainties in the parameters, which will be discussed in more detail in Sec. IV A.

The dynamical range of group parameters in our sample is relatively small – only an order of magnitude in luminosity. To better appreciate the acuteness and significance of the result in Fig. 5, I show in Fig. 6 the same plot, but now including the equivalent data

<sup>3</sup> Reference [32] use the 3.6 micron band, not the K-band as here. Reference [33] [their eq. (6) and Table 2] suggest correcting the K-band value down by about 10 percent to get the stellar value in the 3.6 micron band. This correction is anyhow small compared with the spread we find.

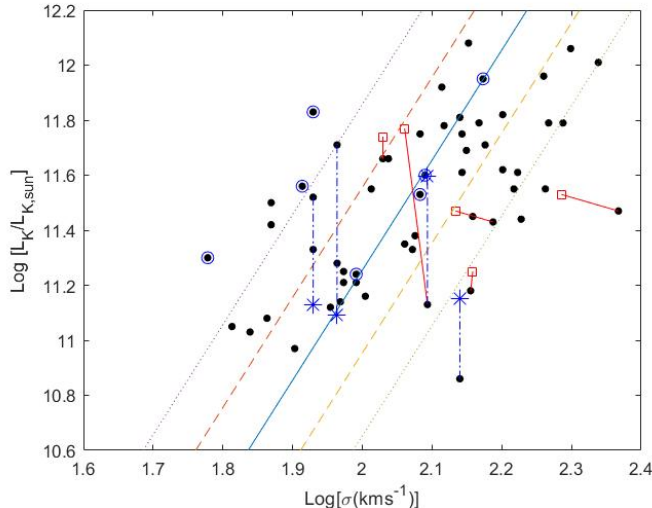


FIG. 5:  $L_K/L_{K,\odot}$  against  $\sigma$  for values from Ref. [13] (filled circles). The positions of the five groups from Paper I that pass our cuts are shown as open (red) squares (with  $L_K/L_{K,\odot}$  and  $\sigma$  from Refs. [11] and [12]). They also appear in our sample, and their positions in the two studies are connected with solid (red) segments. Shown as (blue) asterisks are the distance-corrected positions of the four groups discussed as examples in Sec. IV A; they are connected to the uncorrected positions with (blue) dash-dotted segments. The seven additional groups that I checked and that do not seem to require distance correction (see Sec. IV A) are surrounded by (blue) circles. The parallel lines across the plot show the predictions of eq. (2),  $L_K = (M/L_K)^{-1}(81/4Ga_0)\sigma^4$ , for the sample’s median value,  $M/L_K = 0.7 M_\odot/L_{K,\odot}$  (solid), for half and for twice this value (dashed, upper and lower, respectively), and for a quarter and four times this value (dotted).

for relevant dwarf-spheroidal satellites of Andromeda.<sup>4</sup> “Relevant” means that they are not clearly dominated by an external-field effect (although some are surely still present), and do not show clear signs of rotation – either of which would render the use of eq. (2) invalid. I also took only cases with a large number of observed velocities (when there are two measurements I took the mean of the two), and required that gas does not contribute much to the baryonic mass (otherwise, comparison with stellar  $M/L$  ratios is not meaningful). These include 25 dwarfs from the compilations of Refs. [20, 21]; two dwarfs with good data from Ref. [36]: Cassiopeia III, and Lacerta I;<sup>5</sup> and two dwarfs from Ref. [38]: Cetus and VV 124.

Dwarfs too suffer from systematics that cause artificial

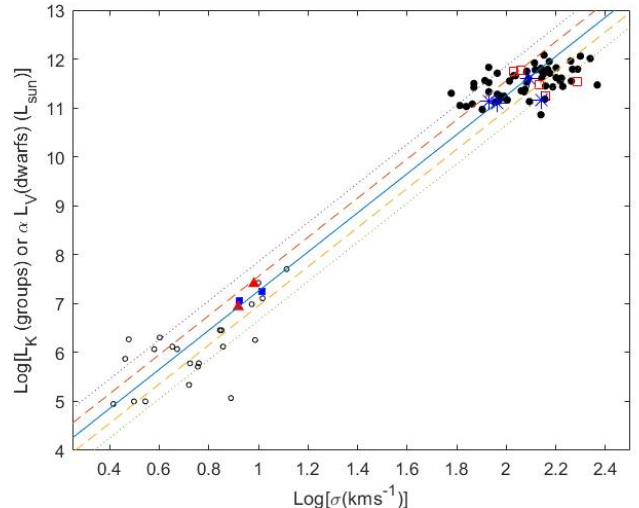


FIG. 6:  $L_K/L_{K,\odot}$  for the groups, and  $\alpha L_V/L_{V,\odot}$  for dwarfs ( $\alpha = 2/0.7$  corrects for the band difference – see the reason below), plotted vs.  $\sigma$ . Groups: filled circles for measured values from Ref. [13], open (red) squares for the five groups from Paper I that pass our cuts, and (blue) asterisks are the corrected positions for the four examples discussed in Sec. IV A (as in Fig. 5). Dwarfs: open circles are for values compiled in Refs. [20, 21] with references given therein; filled (blue) squares are for data from Ref. [36]; filled (red) triangles are for data from Ref. [38]. The lines show the predictions of eq. (2):  $L = (M/L)^{-1}(81/4Ga_0)\sigma^4$ . The solid line is the prediction for  $M/L_K = 0.7 M_\odot/L_{K,\odot}$  for the groups, and for the more appropriate V-band  $M/L_V = 2 M_\odot/L_{V,\odot}$  for the dwarfs (hence the upshift of the dwarf  $L_V$  values by the factor  $\alpha$ ). The dashed lines are for 0.5 (upper) and 2 (lower) times these  $M/L$  values, and the dotted lines are for 0.25 (upper) and 4 (lower) times these values. Error bars for the dwarfs are given in the literature, but not shown here.

scatter, some shared by groups (such as unaccounted-for anisotropies, external-field effects, etc.), some specific to the dwarfs (such as contribution to  $\sigma$  from binaries). But I will not dwell on these here, as I am not testing MOND in dwarfs – this has been done properly in the above references, taking into account rotation, gas content, and possible presence of an external-field effect. Here I only use them as a touchstone for the application of eq. (2).

In light of the discussion in Sec. II B, I also show the results in different forms: Figure 7 shows the ratio  $M_d/M_M$  of the Newtonian, dynamical mass to the MOND mass as a function of  $a_0/g$ . This mass ratio can be viewed as “the mass discrepancy” in the system, and is also the ratio of the observed acceleration,  $g$ , to the Newtonian, gravitational acceleration,  $g_N$ , produced by baryons. Figure 7 thus plots the (very low acceleration end of the) MDAR. This presentation has the advantage that, unlike the  $M - \sigma$  plot, it shows the range of accelerations that are probed in our study. We see that the groups satisfy  $M_d/M_M \approx a_0/g$ , with some scatter, down to values of  $g/a_0 \approx 0.01$ , consistent with the expectation from eq.

<sup>4</sup> From Fig. 6 one may get the impression that the slope within the groups is shallower than the value of 4 dictated by MOND. But this is largely an artifact due to our low- and high-luminosity cutoffs.

<sup>5</sup> These two were already discussed in the context of MOND in Refs. [21, 36, 37]. The third in Ref. [36], Per I, has very large velocity errors.

(8).

Note, however, that while our  $g$  is defined as in eq. (5), with  $\beta = 2$  and  $\bar{R} = R_h$ , the values of  $M_d$  given in Ref. [13] are not calculated from  $\sigma$  and  $R_h$ , with some constant  $\lambda$ , as in our eq. (7); they are calculated in some involved way from the individual velocities and projected positions of the members with measured velocities. So, eq. (8) with these  $M_d$  values is not equivalent to the  $M_M - \sigma$  relation. To see to what extent eq. (7) does approximate the  $M_d$  values with  $\bar{R} = R_h$ , I plot in Fig. 8 the distribution of  $M_d G / R_h \sigma^2$ . We see that the distribution is quite narrow and peaked at  $\approx 10$  (the median is 10.6). Equation (8) is thus a good approximation with  $\bar{R} = R_h$  and  $\beta \lambda^2 \approx 10$ , which makes the coefficient in eq. (8) very near 1. Equation (8) with  $M_d / M_M \approx a_0 / g$  is thus a reasonable approximation to the  $M_M - \sigma$  relation, which underlies the behavior shown in Fig. 7.

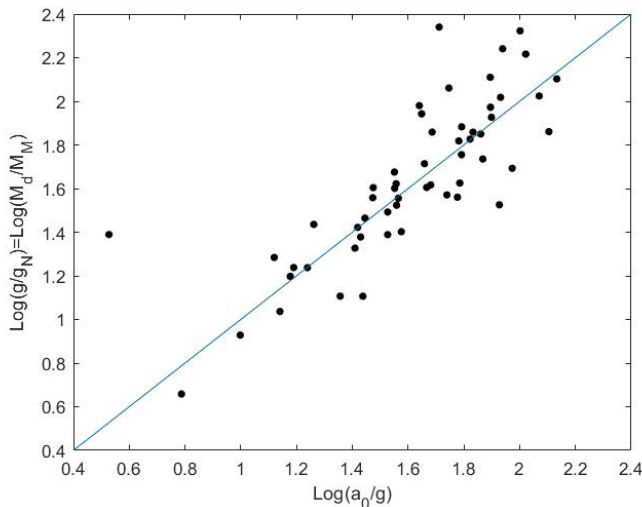


FIG. 7: The MDAR for the groups in the present sample. The Newtonian-to-MOND mass ratio, which can be viewed as the ratio,  $g/g_N$ , of the measured acceleration to the Newtonian, baryonic one – plotted vs.  $a_0/g$ . The equality line – which the MDAR lies very near to for such low accelerations – is also shown.

As a more direct comparison with the MDAR in eq. (6), I show in Fig. 9 a presentation that is *equivalent* to the  $M/L_K$  distribution, i.e. that of  $g/(a_0 g_N)^{1/2}$ , where  $g_N$  is defined in eq. (4) with the choice  $\kappa = 9/4$  [which makes  $\eta = 1$ , in eq. (6), since  $\beta = 2$ ], and the baryonic mass determined from  $L_K$ , taking the median value of  $M/L_K$  to be  $0.7 M_\odot / L_{K,\odot}$  that we found for the  $M_M/L_K$  distribution. A median of 1 is thus enforced with a reasonable values for  $\kappa$ . This figure shows that the distribution of the ratio is narrow.

Figure 10 shows  $\sigma_M/\sigma$  vs.  $R_h$ . We see that there is no significant trend with  $R_h$ . If anything, the agreement with the MOND prediction becomes even tighter at the larger radii, up to  $R_h \approx 700$  Kpc. This is significant in light of the remaining MOND discrepancy

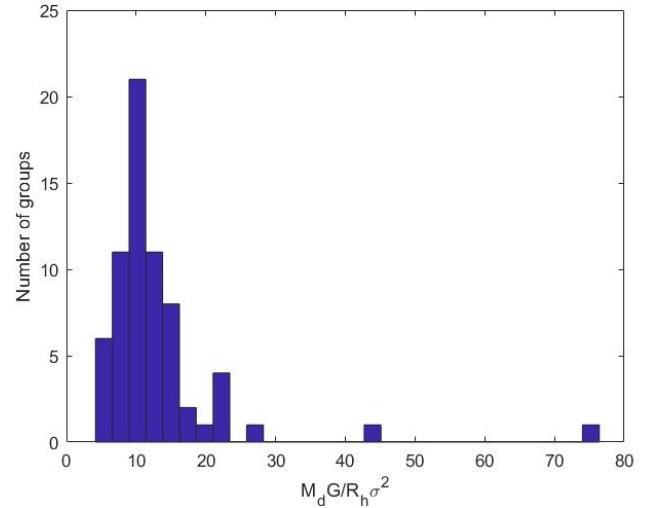


FIG. 8: The distribution of  $M_d G / R_h \sigma^2$  for  $M_d$  and  $\sigma$  values from Ref. [13].

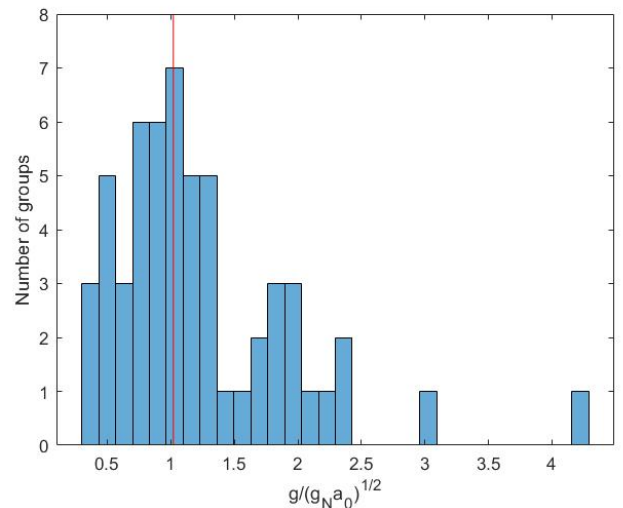


FIG. 9: The distribution of  $g/(a_0 g_N)^{1/2}$ . The median value of 1 – shown as the vertical (red) line – is built in by the choice of normalization of  $g_N$  with factors of order 1.

in cluster cores, which are not larger in size than the high- $R_h$  groups here. The cluster conundrum is sometimes interpreted as some breakdown of MOND at large scales. The lesson from the groups maybe that it is not the size that matters, but some of the other attributes that differentiate between medium-richness groups and clusters. For example, they have very different velocity dispersions (or depth of the potentials [39]). Or, as I discussed in Ref. [27], the culprit might be the prevalent hot, x-ray-emitting gas in clusters and rich groups – absent in large quantities in medium groups – that makes the difference. The idea is that with such gas comes also a yet-undetected baryonic component, dubbed cluster,

baryonic, dark matter. This would account for the remaining MOND discrepancy, and would also account for the observed mass distribution in the “Bullet Cluster”.

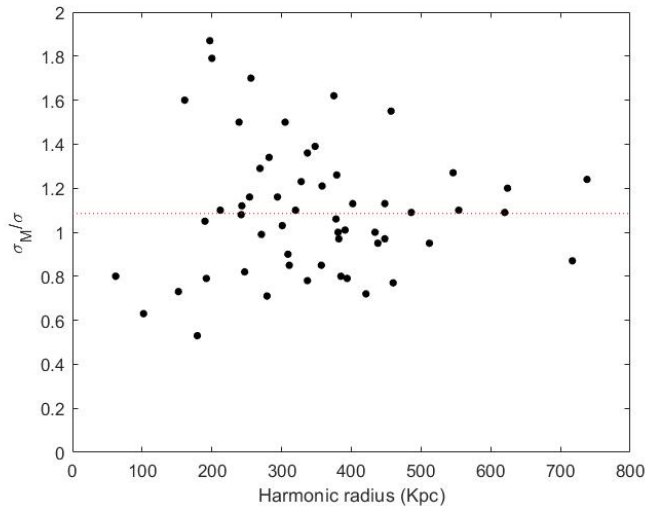


FIG. 10:  $\sigma_M/\sigma$  plotted against the harmonic radius. The median value of  $\sigma_M/\sigma$  is shown.

Figure 11 shows  $\sigma_M/\sigma$  vs.  $N_V$ , where there is no apparent correlation, in particular no apparent decrease in the scatter with increasing  $N_V$ .

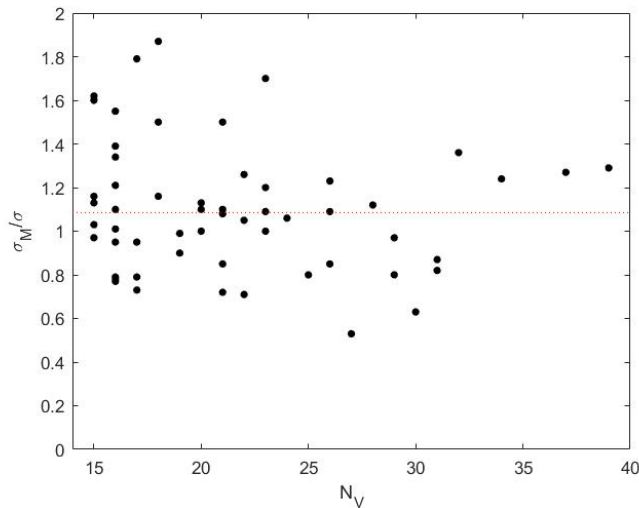


FIG. 11:  $\sigma_M/\sigma$  (with its median indicated) plotted against the number of members with measured velocities.

#### IV. DISCUSSION

I found that intermediate-richness galaxy groups satisfy the deep-MOND relation  $M_M G a_0 = (81/4)\sigma^4$ , with  $M_M/L_K$  values that are characteristic of stars. The

global dynamics of these very-low-acceleration systems are thus accounted for by MOND with no need for dark matter. This contrasts with the very large quantities of dark matter needed in the framework of Newtonian dynamics – typically forty times more dark matter than is observed in stars.

This result is accentuated by our reminder that the same MOND relation is obeyed by dwarf spheroidal galaxies. The groups and dwarfs are two very disparate types of galactic objects, differing by about seven-and-a-half orders of magnitude in baryonic mass, by about two orders in internal velocities, and by three orders in size, and they all lie squarely on the same  $M - \sigma$  relation predicted by MOND.

The scatter we see in Fig. 5 is arguably due partly to genuine variation in the baryonic  $M/L_K$  ratios – due to scatter in stellar  $M/L$  ratios, but also due to the presence of a varying amount of gas (cold and hot), in the member galaxies themselves, and in the intragroup medium, which increases the baryonic values above the stellar values (the mass in the MOND relation is the total baryonic mass). But much scatter surely comes from known (and unknown) systematics, which I discuss below, in Sec. IV A.

This scatter is, in any event, much smaller than the factor of about 40 by which MOND corrects the Newtonian masses.

#### A. Possible systematics

Here I discuss some of the possible systematics that enter the analysis, and the ways they can affect the comparison of the MOND predictions with the observationally deduced quantities.

One important source of error discussed by Ref. [13] is the way they assign distances to the groups. The distances used by Ref. [13] for deducing their group sizes, luminosities, and dynamical masses, and in turn by me to determine  $M_M/L_K$ ,  $\sigma_M$ , etc. are not determined directly. They are all based on the observed mean recession velocities with respect to the local group, and assuming a strict Hubble flow, with  $H_0 = 73 \text{ km s}^{-1} \text{ Mpc}^{-1}$ . As discussed in Ref. [13], this can clearly lead, in some cases, to systematic errors in all the above mentioned system parameters. To quote Ref. [13]: “The disadvantage of our algorithm, where the distance of a group is determined by the mean radial velocity of its galaxies, is most pronounced in the regions with large peculiar motions. Some groups we identified in the Virgo cluster core are, most probably, false groups, rather than physical subsystems in the Virgo cluster.”

This issue is particularly acute for (nearby) groups with low Hubble velocities – which Ref. [13] largely excluded from their list. It is also acute when the group resides in a region characterized by high peculiar velocities, such as in a cluster environment, which can modify the recession velocity.



I already mentioned in Sec. II C the group “NGC 4216”, which has a recession speed of  $55 \text{ km s}^{-1}$ , but is “located in the Virgo cluster core”, and fell prey to this error.

As mentioned in Sec. III, five of the groups in the present sample appear in the samples used in Paper I, and pass out cuts. They were assigned different parameter values in the more recent catalogs of Refs. [11, 12], used in Paper I. These latter assigned distances based on more direct measures. These differences are evident in Fig. 5, where they are compared. We see that the assigned distances (hence  $L_K$ ) have been updated but also the values of  $\sigma$  changed. For example, “NGC 3379” has the highest  $M_M/L_K = 12.63 M_\odot/L_{K,\odot}$  in our sample (and  $\sigma_M/\sigma = 0.53$ ), which is based on Ref. [13] giving for it  $\sigma = 233 \text{ km s}^{-1}$  (with  $N_V = 27$ ). The more recent Ref. [11] gives it  $\sigma = 193 \text{ km s}^{-1}$  (with  $N_V = 36$ ), which, with also an increase in  $L_K$ , gives this group  $M_M/L_K = 5.2 M_\odot/L_{K,\odot}$  ( $\sigma_M/\sigma = 0.66$ ).

Another of these five groups is the “NGC 3607” (Leo II) group. It has a recession speed of  $V_{LG} = 960 \text{ km s}^{-1}$ , which gives a redshift distance of 13 Mpc. Reference [11], used in Paper I, assigned to it a distance of 25 Mpc, which gave in Paper I,  $M_M/L_K = 0.38 M_\odot/L_{K,\odot}$  ( $\sigma_M/\sigma = 1.28$ ). (This shows as the largest shift in Fig. 5.) Moreover, the distance given in Ref. [40] for this group is  $\approx 22.2$  Mpc, which would correct the  $M_M/L_K = 2.2 M_\odot/L_{K,\odot}$  ( $\sigma_M/\sigma = 0.82$ ) in Table I to  $M_M/L_K = 0.83 M_\odot/L_{K,\odot}$  ( $\sigma_M/\sigma = 1.05$ ).

Since the adopted distances may pose such a problem, I checked eleven of the groups to see to what extent distances determined from nonredshift methods (Cepheids, Tully-Fisher, surface-brightness fluctuations, etc.) differ from those adopted in Ref. [13]. I checked seven outliers and four groups whose  $M_M/L_K$  are near the median value of  $0.7 M_\odot/L_{K,\odot}$ . I found that for the latter four, nonredshift distances are consistent with the ones adopted, so their near-median  $M_M/L_K$  is unaltered. Of the seven outliers, three do not seem to require a distance correction (“NGC 3801”, “NGC 0488”, and “NGC 891”).

Four of the outliers do require corrections if the nonredshift distances are correct. One is the above mentioned “NGC 3607”. Another, less severe case (not appearing in Paper I), is “NGC 3031” (M81), with our second highest  $M_M/L_K$  value. Based on the recession speed of  $V_{LG} = 193 \text{ km s}^{-1}$ , the redshift-based distance is 2.64 Mpc. But its Cepheid distance is 3.7 Mpc, reducing  $M_M/L_K$  by a factor of 0.51, from 6.3 in Table I to 3.2 (and corrects to  $\sigma_M/\sigma = 0.75$ ).

Yet another is “NGC 4254” (M99), which has  $M_M/L_K = 0.18 M_\odot/L_{K,\odot}$ . Its recession speed in Ref. [13] is  $2296 \text{ km s}^{-1}$ , which gives a Hubble-flow distance of 31.45 Mpc. However, its directly measured distance as given in NASA Extragalactic Database is  $D = 15.4 \pm 1.7$  Mpc. With this distance, we should correct to  $M_M/L_K = 0.75$  (and  $\sigma_M/\sigma = 1.07$ ).

And yet another is “NGC 4527”, whose Hubble-flow distance is  $D = 22$  Mpc, but it is in the Virgo cluster

in projection; so could have a large peculiar component. Indeed, the Cepheid distance to NGC 4527 (the galaxy) is  $14 \pm 1.6$  Mpc [41]. This requires correcting the MOND  $M/L$  value in Table I by a factor 2.5, from the smallest  $M_M/L_K = 0.2 M_\odot/L_{K,\odot}$  ( $\sigma_M/\sigma = 1.5$ ) to  $M_M/L_K = 0.5 M_\odot/L_{K,\odot}$  ( $\sigma_M/\sigma = 1.2$ ).

All eleven examples are also shown in Fig. 5.

While, generally, the Hubble-flow distances are rather reliable, we see that at least some of the scatter must be due to this sometimes-inaccurate distance assignment.

Another source of uncertainty, as mentioned already, is the possible presence in member galaxies or the intra-group space, of additional baryons, such as cold, warm, or hot gas. This may explain some of the higher-than stellar MOND  $M_M/L_K$  values.

Departure from the velocity isotropy that is assumed in all analyses, when we replace the three-dimensional velocity dispersion by  $\sqrt{3}\sigma$ , also leads to artificial scatter in the observed  $M_M - \sigma$  relation. Such anisotropies are surely present, but it is difficult to quantify them without measuring proper motions as well as radial velocities.

In the analyses of whole samples, such as here, such unaccounted-for anisotropies are expected to lead to increased scatter, not to systematic shifts. But one has to be careful not to put too much weight on apparent departures of this or that individual case, be it a group or another “pressure-supported” system.

Another possible source of systematics is departure from virialization. Artificially elevated values of  $\sigma_M/\sigma$  can also be caused, e.g., by the system not yet having reached virialization. I show in Table I a measure of the dynamical time in the group,  $\tau_d \equiv R_h/\sigma$ . Its values are fractions of the Hubble time, but not exceedingly smaller. It is not clear what is the limit on  $\tau_d$  necessary for virialization (and this may anyway vary from system to system). We expect large dynamical times, of the order of the Hubble time to indicate that the system is still collapsing towards virial equilibrium, and hence has a lower-than-virial value of  $\sigma$  resulting in  $\sigma_M/\sigma > 1$ . We see in Fig. 12, some correlation of high  $\sigma_M/\sigma$  values with high  $\tau_d$  values. But it is not clear that this is not an artifact of our definitions, which imply that  $\sigma_M/\sigma \propto \tau_d(L_K^{1/4}/R_h)$  should hold exactly. So, if, for example,  $L_K^{1/4}/R_h$  is not correlated with  $\tau_d$ , any scatter in  $\sigma$  around the correct value will create such a correlation artificially.

### 1. External-field effect?

In MOND, an additional source of deviation from relation (2) is the possible presence of an external-field effect (EFE) due to external accelerations to which the groups are subject (see Refs. [1, 20, 21, 42] for a few of many treatments of this effect for pressure-supported systems).

The description of the effect is relatively simple only when the (MOND) external acceleration,  $g_{ex} \gg g_{in} \approx g$ ,  $g_{in}$  is the (MOND) internal acceleration. In the opposite case the effect is negligible, and it is rather complicated

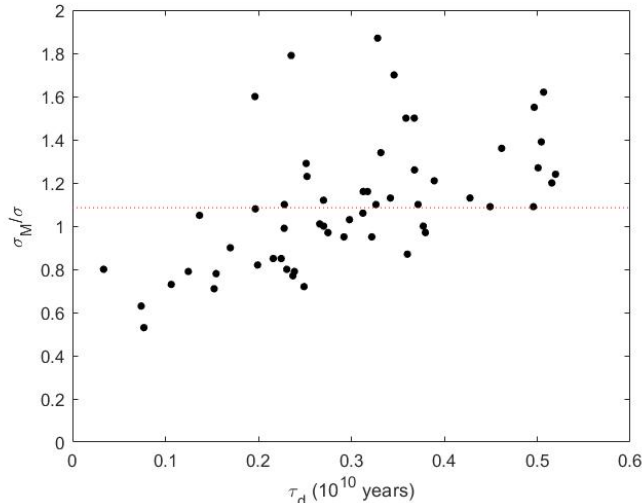


FIG. 12:  $\sigma_M/\sigma$  plotted against the dynamical time.

to account for when  $g_{ex} \approx g_{in}$ , as might be the case for some of our groups. Equation (2) – which assumes that the system is isolated – underestimates the baryonic mass when an EFE is present, i.e., when  $g_{ex} \ll g_{in}$ . It then leads to artificially low  $M_M/L_K$  values, or high  $\sigma_M/\sigma$  values.<sup>6</sup>

For  $g_{ex} \gg g_{in}$  the effect works as follows: Suppose the  $\sigma$  value given in Ref. [13] is  $\sigma = \sigma_{Me}$ , where  $\sigma_{Me}$  is the correct dispersion in all regards which would be exactly obtained from a MOND prediction that includes the EFE, using  $L_K$  with a correct  $M/L_K = 1 M_\odot/L_{K,\odot}$ , while  $\sigma_{Mi}$  is what I calculate as  $\sigma_M$  assuming isolation. Then, using eq. (6) it can be shown that

$$\frac{\sigma_{Mi}}{\sigma_{Me}} = \eta^{1/2} \left( \frac{g_{ex}}{g} \right)^{1/4} \approx \left( \frac{g_{ex}}{g} \right)^{1/4} \approx \frac{g_{ex}^{1/2}}{(g_N a_0)^{1/4}}, \quad (10)$$

where  $\eta \approx 1$  is defined in eq. (6), and  $g$  is related to  $\sigma$  by eq. (5). Table I shows the values of  $g \equiv 2\sigma^2/R_h$ . For many groups  $g$  is low enough – a few percents of  $a_0$ , or even less – that an EFE may be present due to surrounding structures. This is because the amplitude of the varying ambient acceleration field may be of that order. It can be estimated, e.g., as the acceleration to typical peculiar velocities of  $\approx 300 \text{ km s}^{-1}$  during the Hubble time. For example, Ref. [43] estimates for the local groups  $g_{ex} \approx 2.2 \times 10^{-2} a_0$ .

If all else was exact, with no measurement errors, and no departure from any of our assumptions, except that of isolation, then departures of  $\sigma_M/\sigma$  from unity would only be due to the EFE, and be given, for  $g_{ex} \gg g$ , by

eq. (10). Then, if  $g_{ex}$  is not correlated with  $g$ , we would expect  $\sigma_M/\sigma$  to be unity for  $g \ll g_{ex}$  and broadly behave as  $g^{-1/4}$  at very small  $g$  values, with scatter that comes from that in  $g_{ex}$  from system to system. We can then look for such a correlation.

However, as in the case of the dynamical time, correlations of  $\sigma_M/\sigma$  with  $g$  can also result artificially. From our definitions in Sec. IIB we have exactly

$$\frac{\sigma_M}{\sigma} = \eta^{1/2} \frac{(a_0 g_N)^{1/4}}{g^{1/2}}. \quad (11)$$

In other words, in terms of the quantities from Ref. [13] that we use, and our assumptions that go into the calculation of  $\sigma_M$  and  $g$  (e.g., that  $M/L_K = 1$ ) we have, by the definitions,  $\sigma_M/\sigma \propto L_K^{1/4} R_h^{-1/2} g^{-1/2}$ . So, for example, if there was no EFE, and all measurements were correct except that the  $\sigma$  values depart from their correct values, with no correlation with  $g_N$ , then eq. (11) tells us to expect  $\sigma_M/\sigma \propto g^{-1/2}$ , with scatter reflecting that in  $g_N$ . This would produce an artificial correlation between  $\sigma_M/\sigma$  and  $g$ . (Of course, if all quantities are exact, MOND predicts that  $g$  is correlated with  $g_N$ , so that  $\sigma_M/\sigma = 1$  for all groups.)

Figure 13 shows  $\sigma_M/\sigma$  vs.  $g$  for the groups. Also shown are a line of slope  $-1/4$  following eq. (10), with  $g_{ex} = 3 \times 10^{-2} a_0$ , for  $g \leq g_{ex}$ , and a line with slope  $-1/2$  crossing the first line at  $g = g_{ex}$ .

We see clearly that indeed there is a correlation with the unexpectedly high  $\sigma_M/\sigma$  values occurring for the lowest values of  $g$ , and they decrease with increasing  $g$ . However, this correlation follows more closely eq. (11); so much of it may well be an artifact. It is difficult to judge whether some of the correlation is due to the presence of an EFE.

Because  $\sigma$  enters directly the definition of  $g$ , which may introduce artificial correlation, it may be more informative to look for a correlation between  $\sigma_M/\sigma$  and  $g_N$ , as in the last equality in eq. (10), since  $g_N$  is derived from only  $L_K$  and  $R_h$ , and does not use  $\sigma$ . This is shown in Fig. 14, with the *asymptotic* ( $g \ll g_{ex}$ ) lines of slope  $-1/4$  describing the last near equality in eq. (10), with  $g_{ex} = (2, 3) \times 10^{-2} a_0$ . No clear correlation is seen.

It is possible to hide the presence of an EFE in this plot; but unless the scatter in  $g_{ex}$  is very large it seems that most of the scatter in  $\sigma_M/\sigma$  is not caused by an EFE, but by other causes, such as discussed above. In particular, we see that the largest values of  $\sigma_M/\sigma$  do not occur for the lowest  $g_N$  groups.

There is a clear potential in the group dynamics to detect the EFE, but in the present analysis, I have not been able to establish its presence, possibly because it is masked by other, more dominant sources of scatter. It is worthwhile investigating this issue further because the EFE is peculiar to MOND, and should not appear in the dark-matter paradigm and could be a discriminating phenomenon. A more thorough analysis may require going beyond statistical arguments and considering individual groups in the context of their environments.

<sup>6</sup> MOND predicts an acceleration discrepancy  $\approx a_0/\bar{g}$ , with  $\bar{g}$  the larger of the internal and external accelerations. Assuming isolation in effect uses  $\bar{g} = g_{in}$  instead of the larger  $g_{ex}$ .

I thank Indranil Banik, Pavel Kroupa, and Stacy McGaugh for comments on the manuscript.

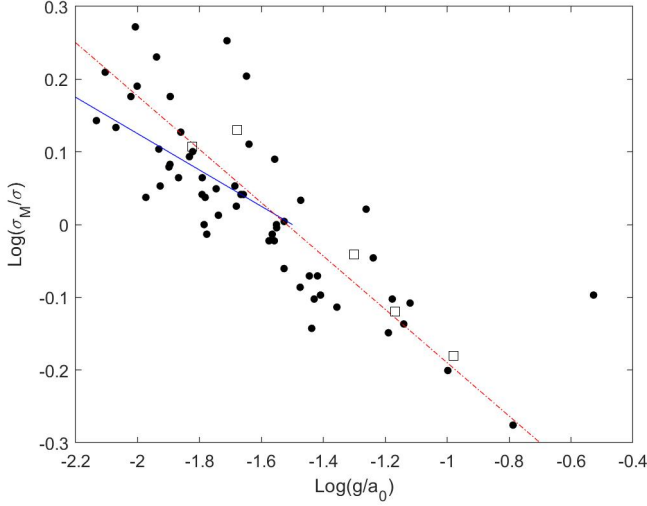


FIG. 13:  $\sigma_M/\sigma$  plotted against  $g/a_0$  (filled circles). The position of the five groups from Paper I are shown as squares. The solid (blue) line has a slope of  $-1/4$  and follows eq. (10) with  $g_{ex} = 3 \times 10^{-2} a_0$ . The dash-dotted (red) line has a slope of  $-1/2$ , as in eq. (11).

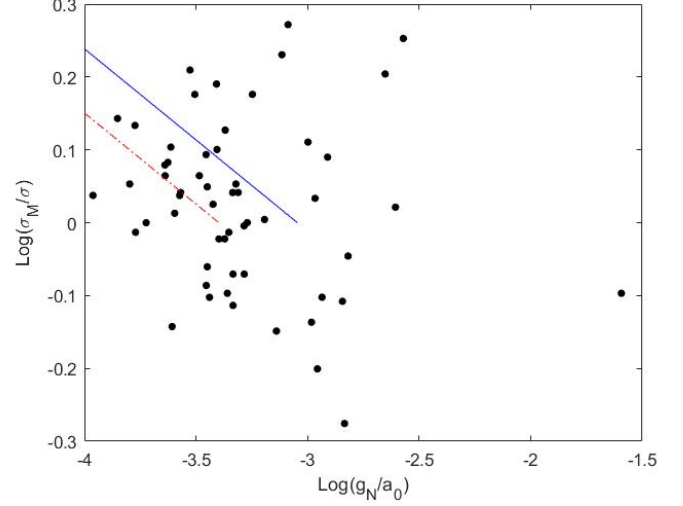


FIG. 14:  $\sigma_M/\sigma$  plotted against  $g_N/a_0$  (filled circles). Lines with a slope of  $-1/4$  that follow the asymptotic ( $g \ll g_{ex}$ ), last near-equality in eq. (10), are also shown with  $g_{ex} = 3 \times 10^{-2} a_0$  (blue, solid) and  $g_{ex} = 2 \times 10^{-2} a_0$  (red, dash dotted).

- 
- [1] M. Milgrom, *Astrophys. J.* 270, 365 (1983).  
[2] B. Famaey and S. McGaugh, *Liv. Rev. Rel.* 15, 10 (2012).  
[3] M. Milgrom, *Scholarpedia* 9(6), 31410 (2014).  
[4] P. Kroupa, arXiv:1610.03854 (2016).  
[5] W. Oehm and P. Kroupa, arXiv:1811.03095 (2018).  
[6] M. Milgrom, *Phys. Rev. Lett.* 111, 041105 (2013).  
[7] M.M. Browner et al., *MNRAS* 466, 2547 (2017).  
[8] F. Lelli et al., *Astrophys. J.* 836, 152 (2017).  
[9] M. Milgrom, *Phys. Rev. D* 98, 104036 (2018).  
[10] I.D. Karachentsev, O.G. Kashibadze, and V.E. Karachentseva, *Astrophys. Bull.* 72, 111 (2017).  
[11] I.D. Karachentsev, O.G. Nasonova, and V.E. Karachentseva, *Astrophys. Bull.* 70, 1 (2015).  
[12] I.D. Karachentsev, V.E. Karachentseva, and O.G. Nasonova, *Astrophys.* 57, 457 (2014).  
[13] D. Makarov and I. Karachentsev, *MNRAS* 412, 2498 (2011).  
[14] M. Milgrom, *Astrophys. J.* 270, 384 (1983).  
[15] M. Milgrom, *Astrophys. J. Lett.* 496, L89 (1998).  
[16] M. Milgrom, *Astrophys. J. Lett.* 577, L75 (2002).  
[17] R.B. Tully et al., *Astrophys. J.* 569, 573 (2002).  
[18] R. Scarpa, arXiv:astro-ph/0302445 (2003).  
[19] M. Milgrom, *Phys. Rev. D* 89, 024016 (2014).  
[20] S. McGaugh and M. Milgrom, *Astrophys. J.* 766, 22 (2013).  
[21] S. McGaugh and M. Milgrom, *Astrophys. J.* 775, 139 (2013).  
[22] R. Durazo, et al., *Astrophys J.* 863, 107 (2018).  
[23] M. Milgrom, *Astrophys. J.* 698, 1630 (2009).  
[24] M. Milgrom, *Ann. Phys.* 229, 384 (1994).  
[25] M. Milgrom, *MNRAS* 437, 2531 (2014).  
[26] G.W. Angus, B. Famaey, and D.A. Buote, *MNRAS* 387, 1470 (2008).  
[27] M. Milgrom, *New Astron. Rev.* 51, 906 (2008).  
[28] T. Richtler et al., *Astron. Astrophys.* 531, A119 (2011).  
[29] M. Hilker et al., *Astron. Astrophys.* 619, A70 (2018).  
[30] K.W. Wong et al., *Astrophys. J.* 829, 49. (2016).  
[31] H. Roussel, R. Sadat, and A. Blanchard, *Astron. Astrophys.* 361, 429 (2000).  
[32] P. Li, et al. *Astron. Astrophys.* 615, A3 (2018).  
[33] S.H. Oh, et al., *Astron. J.* 136, 2761 (2008).  
[34] R.H. Sanders and M.A.W Verheijen, *Astrophys. J.* 503, 97 (1998).  
[35] E.F. Bell and R.S. de Jong, *Astrophys. J.* 550, 212 (2001).  
[36] M.N. Martin et al., *Astrophys. J. L.* 793, L14 (2014).  
[37] M.S. Pawlowski and S.S. McGaugh, *MNRAS* 440, 908 (2014).  
[38] E.N. Kirby et al., *MNRAS* 439, 1015 (2014).  
[39] H. Zhao and B. Famaey, *Phys. Rev. D* 86, 067301 (2012).  
[40] J.P. Brodie et al., *Astrophys. J.* 796, 52 (2014).  
[41] A. Saha et al., *Astrophys. J.* 551, 973 (2001).  
[42] H. Haghi et al., *MNRAS* 395, 1549 (2009).  
[43] I. Banik, D. O’Ryan, and H.S. Zhao, *MNRAS* 477, 4768 (2018).

TABLE I: The 67 groups cataloged in Ref. [13], with number of members with measured radial velocities  $N_V \geq 15$  (ordered by decreasing  $N_V$ ). Groups marked with \* are not included in the analysis, for reasons explained in the text. Observed parameters with Newtonian, dynamical masses and mass-to-light ratios as derived in Ref. [13] (columns 1-7), and MOND-related quantities that are derived here (columns 8-13). (1) group name; (2) number of members with measured line-of-sight velocity; (3) line-of-sight velocity dispersion in  $\text{km s}^{-1}$ ; (4) harmonic radius in Kpc; (5)  $\log_{10}(L_K/L_{K,\odot})$ ; (6) dynamical mass  $\log_{10}(M_d/M_\odot)$ ; (7) dynamical  $M_d/L_K$  in solar units; (8) MOND velocity dispersion calculated from eq. (2), assuming baryonic  $M_b/L_K = 1 M_\odot/L_{K,\odot}$ , in  $\text{km s}^{-1}$ ; (9) the ratio  $\sigma_M/\sigma$ ; (10) MOND mass from  $\sigma$  using eq. (2), in units of  $10^{12}M_\odot$ ; (11) baryonic, MOND  $M_M/L_K$  in solar units; (12) a measure of the dynamical time,  $\tau_d \equiv R_h/\sigma$ , in units of  $10^{10}$  years; (13) A measure of the acceleration in the group,  $g \equiv 2\sigma^2/R_h$ , in units of  $10^{-2}a_0$ .

Group	$N_V$	$\sigma$	$R_h$	$\lg L_K$	$\lg M_d$	$M_d/L_K$	$\sigma_M$	$\sigma_M/\sigma$	$M_{M,12}$	$M_M/L_K$	$\tau_{d,10}$	$10^2 g/a_0$
(1)	(2)	(3)	(4)	(5)	(6)	(7)	(8)	(9)	(10)	(11)	(12)	(13)
NGC4472*	355	291	696	12.44	14.14	50	216	0.74	9.07	3.29	0.24	6.55
NGC3311*	139	426	520	12.51	14.29	60	225	0.53	41.66	12.87	0.12	18.78
NGC4696*	116	303	690	12.5	14.13	43	224	0.74	10.66	3.37	0.23	7.16
NGC1316*	111	244	454	12.3	13.94	44	200	0.82	4.48	2.25	0.19	7.06
NGC4261*	87	276	358	11.99	13.7	51	168	0.62	7.34	7.51	0.13	11.45
NGC5846*	74	228	395	11.8	13.64	69	150	0.66	3.42	5.42	0.17	7.08
NGC3992*	72	120	452	11.68	13.33	45	140	1.16	0.26	0.55	0.38	1.71
NGC5371*	55	195	455	12.07	13.69	42	175	0.9	1.83	1.56	0.23	4.5
NGC3223*	53	404	368	12.13	14.31	151	181	0.45	33.7	24.98	0.09	23.86
NGC5044*	52	245	480	11.96	13.72	58	164	0.67	4.56	5	0.2	6.73
NGC5746	39	107	269	11.66	13.2	35	138	1.29	0.17	0.36	0.25	2.29
NGC4697	37	109	546	11.66	13.27	41	138	1.27	0.18	0.39	0.5	1.17
NGC3100	34	142	738	12.08	13.57	31	176	1.24	0.51	0.43	0.52	1.47
NGC4636	32	73	337	11.08	12.58	32	99	1.36	0.04	0.3	0.46	0.85
NGC3607	31	124	247	11.13	13.08	89	102	0.82	0.3	2.22	0.2	3.35
NGC4501	31	199	717	12.06	13.79	54	174	0.87	1.98	1.73	0.36	2.97
NGC3031	30	138	102	10.86	12.59	54	87	0.63	0.46	6.33	0.07	10.04
NGC1553	29	185	62	11.79	13.56	59	149	0.8	1.48	2.4	0.03	29.7
NGC4105	29	139	382	11.61	13.23	42	134	0.97	0.47	1.16	0.27	2.72
NGC4631	28	90	243	11.12	12.98	72	101	1.12	0.08	0.63	0.27	1.79
NGC3379	27	233	179	11.47	13.23	58	124	0.53	3.73	12.63	0.08	16.32
NGC3923	26	159	357	11.62	13.33	51	135	0.85	0.81	1.94	0.22	3.81
ESO507-025	26	130	328	11.92	13.18	18	160	1.23	0.36	0.43	0.25	2.77
NGC5078	26	138	620	11.81	13.48	47	151	1.09	0.46	0.71	0.45	1.65
NGC1407	25	167	385	11.61	13.32	51	134	0.8	0.98	2.42	0.23	3.9
NGC1395	24	121	378	11.53	13.05	33	128	1.06	0.27	0.8	0.31	2.08
NGC4039	23	74	256	11.5	12.82	21	126	1.7	0.04	0.12	0.35	1.15
NGC4303	23	115	434	11.35	12.97	42	116	1	0.22	0.99	0.38	1.64
NGC4535	23	121	624	11.75	13.36	41	145	1.2	0.27	0.48	0.52	1.26
NGC4753	23	98	486	11.21	12.76	35	107	1.09	0.12	0.72	0.5	1.06
NGC0988	22	103	379	11.55	12.98	27	130	1.26	0.14	0.4	0.37	1.51
NGC1332	22	183	279	11.55	13.39	69	130	0.71	1.42	4	0.15	6.46
NGC7176	22	139	190	11.75	13.11	23	145	1.05	0.47	0.84	0.14	5.47
NGC4373	21	149	554	11.95	13.4	28	163	1.1	0.62	0.7	0.37	2.16
NGC5322	21	169	421	11.44	13.12	48	122	0.72	1.03	3.75	0.25	3.65
NGC3877	21	65	239	11.05	12.57	33	97	1.5	0.02	0.2	0.37	0.95
NGC3894	21	123	242	11.6	13.02	26	133	1.08	0.29	0.73	0.2	3.36
NGC2911	21	144	311	11.45	13.2	56	122	0.85	0.54	1.93	0.22	3.59
NGC4111	20	93	212	11.14	12.69	35	102	1.1	0.09	0.69	0.23	2.19
NGC5011	20	131	448	11.78	13.43	45	148	1.13	0.37	0.62	0.34	2.06
NGC5557	20	141	381	11.69	13.3	41	141	1	0.5	1.02	0.27	2.81
NGC3610	19	119	271	11.38	13.08	50	118	0.99	0.25	1.06	0.23	2.81
NGC6868	19	182	309	11.96	13.38	26	164	0.9	1.39	1.52	0.17	5.77
NGC0891	18	60	197	11.3	12.64	22	112	1.87	0.02	0.08	0.33	0.98
NGC4527	18	85	305	11.52	12.93	26	127	1.5	0.07	0.2	0.36	1.27
NGC5473	18	94	294	11.25	12.75	32	109	1.16	0.1	0.56	0.31	1.62
NGC0488	17	85	200	11.83	13.16	21	152	1.79	0.07	0.1	0.24	1.94
ESO320-031	17	150	438	11.71	13.33	42	142	0.95	0.64	1.25	0.29	2.76
NGC5363	17	143	152	11.18	12.76	38	105	0.73	0.53	3.49	0.11	7.24
NGC4321	17	165	394	11.55	13.35	63	130	0.79	0.94	2.64	0.24	3.72
NGC0524	16	147	391	11.79	13.16	23	149	1.01	0.59	0.96	0.27	2.97
NGC3627	16	154	192	11.43	13.05	42	121	0.79	0.71	2.64	0.12	6.65
NGC3945	16	92	358	11.28	12.93	45	111	1.21	0.09	0.48	0.39	1.27

TABLE I: Continue

Group	$N_V$	$\sigma$	$R_h$	$\lg L_K$	$\lg M_d$	$M_d/L_K$	$\sigma_M$	$\sigma_M/\sigma$	$M_{M,12}$	$M_M/L_K$	$\tau_{d,10}$	$10^2 g/a_0$
(1)	(2)	(3)	(4)	(5)	(6)	(7)	(8)	(9)	(10)	(11)	(12)	(13)
NGC4151	16	69	348	11.03	12.56	34	96	1.39	0.03	0.27	0.5	0.74
NGC4216*	16	52	23	8.6	11.24	437	24	0.46	0.01	23.23	0.04	6.33
NGC4254	16	92	457	11.71	13.28	37	142	1.55	0.09	0.18	0.5	1
NGC4666	16	98	320	11.24	12.95	51	108	1.1	0.12	0.67	0.33	1.61
NGC4936	16	194	460	11.79	13.36	37	149	0.77	1.79	2.91	0.24	4.4
NGC5090	16	218	337	12.01	13.74	54	169	0.78	2.86	2.79	0.15	7.59
NGC5982	16	159	512	11.82	13.31	31	151	0.95	0.81	1.22	0.32	2.66
NGC3801	15	82	161	11.56	12.7	14	130	1.6	0.06	0.16	0.2	2.25
NGC4224	15	118	448	11.33	12.95	42	114	0.97	0.25	1.15	0.38	1.67
NGC4258	15	80	254	10.97	12.45	30	93	1.16	0.05	0.56	0.32	1.36
NGC4993	15	74	375	11.42	12.44	10	120	1.62	0.04	0.14	0.51	0.79
NGC5128	15	94	402	11.21	12.52	20	107	1.13	0.1	0.61	0.43	1.18
NGC5198	15	101	301	11.16	12.69	34	104	1.03	0.13	0.91	0.3	1.82